Laboratory technology and cosmochemistry

Ernst K. Zinner[a,1], Frederic Moynier[b], and Rhonda M. Stroud[c]

[a]*Laboratory for Space Sciences and Physics Department, and* [b]*Department of Earth and Planetary Sciences, Washington University, St. Louis, MO 63130; and* [c]*Materials Science and Technology Division, Code 6360, Naval Research Laboratory, Washington, DC 20375*

Edited by Mark H. Thiemens, University of California at San Diego, La Jolla, CA, and approved March 14, 2011 (received for review October 12, 2010)

Recent developments in analytical instrumentation have led to revolutionary discoveries in cosmochemistry. Instrumental advances have been made along two lines: (*i*) increase in spatial resolution and sensitivity of detection, allowing for the study of increasingly smaller samples, and (*ii*) increase in the precision of isotopic analysis that allows more precise dating, the study of isotopic heterogeneity in the Solar System, and other studies. A variety of instrumental techniques are discussed, and important examples of discoveries are listed. Instrumental techniques and instruments include the ion microprobe, laser ablation gas MS, Auger EM, resonance ionization MS, accelerator MS, transmission EM, focused ion-beam microscopy, atom probe tomography, X-ray absorption near-edge structure/electron loss near-edge spectroscopy, Raman microprobe, NMR spectroscopy, and inductively coupled plasma MS.

microanalysis | extraterrestrial materials

Cosmochemistry is concerned with the study of the Solar System (SS), its formation, its history, and the processes that shaped the planets. This is mainly accomplished through the analysis of extraterrestrial samples, astronomical observations from Earth and space, and in situ measurements by robotic spacecrafts. The latter is the topic of a separate chapter; this chapter is concerned with the question of how recent advances in laboratory instrumentation have led to revolutionary discoveries in cosmochemistry.

The study of extraterrestrial samples includes the analysis of meteorites (from asteroids, Mars, and the Moon), lunar samples (returned by Apollo), micrometeorites (1), interplanetary dust particles (IDPs) (2, 3), samples returned from comets (Stardust) (4), asteroids (HAYABUSA) (5), and samples from the Sun (Genesis) (6).

Throughout the 20th century, continuous development of analytical instrumentation has led to a deep understanding of how the SS formed, what material contributed to its formation, what processes took place in its early history, and what was the time scale. An important step in the development of instrumental capabilities was the Apollo Program. Funding for instrumentation for the analysis of returned lunar samples led to analytical advances that, in turn, resulted in pathbreaking discoveries in other fields. Examples are the discovery of ^{16}O excesses in Ca-Al–rich inclusions (CAIs) (7) and evidence for the initial presence of ^{26}Al in the early SS (ref. 8; see also ref. 9).

The last two decades have seen a plethora of instrumental developments that have led to revolutionary discoveries. The whole field of the analysis of extraterrestrial materials has grown to an extent and involves so many different analytical techniques that a detailed survey is completely out of the question in the framework of this paper. In our treatment, we will emphasize the impact of instrumentation on cosmochemistry. This will exclude many conventional techniques, such as X-ray analysis in the electron microprobe and SEM, neutron activation analysis, conventional X-ray fluorescence, and X-ray diffraction analysis, which are important to cosmochemistry but are discussed extensively elsewhere.

Recent progress in instrumental developments has mainly been made along two lines.

i) Increase in spatial resolution and sensitivity of detection, allowing for the study of increasingly smaller samples such as IDPs, stellar condensates (presolar grains), and returned material from the Stardust and Genesis missions. Examples of instruments include the transmission EM (TEM), secondary ion MS (NanoSIMS), resonance ionization MS (RIMS), Auger probe, atom probe, and synchrotron X-ray fluorescence (μ-XRF).

ii) Increase in the precision of isotopic analysis that allows for more precise dating, the study of isotopic heterogeneity in the SS, and other studies. An example is multicollector inductively coupled plasma MS (MC-ICP-MS).

In some cases, one can achieve both high precision at fairly high spatial resolution. Examples are ion microprobe analysis of the Al-Mg system and O-isotopic measurements of chondrules and CAIs with large-sector ion microprobes and Faraday cup detection.

The small amounts of material returned by the Stardust and Genesis missions have not only provided motivation to try new analysis and sample handling (10) techniques but have fostered collaborations and combination of a multitude of different analytical instruments. As an example, the reader is referred to a special issue of *Meteoritics and Planetary Science* (11) that is devoted to the analysis of material returned by the Stardust mission.

In the following, we will shortly describe various instrumental techniques and discuss important results obtained by their application.

Ion Microprobe

The ion microprobe has become the most important instrument for the isotopic analysis of small samples (12, 13). It uses SIMS. In this technique, a primary ion beam (O or Cs) of typically 15–20 keV energy is focused into a small spot onto the sample. Of the atoms sputtered by the primary beam bombardment, a certain fraction (the ionization efficiency strongly depends on the element) is emitted as ions, and these secondary ions are analyzed in a double-focusing magnetic sector mass spectrometer either by single ion counting in electron multipliers or by charge measurement in Faraday cups (FC).

One of the major applications of the ion microprobe is the isotopic analysis of presolar grains (14, 15). These grains, found in primitive meteorites, are bona fide stardust. They condensed in the expanding atmospheres of late-type stars [red giant branch (RGB) and asymptotic giant branch (AGB) stars] and in the ejecta from supernova (SN) explosions. They carry the isotopic compositions of their stellar sources and thus, give information about stellar nucleosynthesis and the isotopic evolution of the Galaxy. The ion microprobe makes it possible to

Author contributions: E.K.Z., F.M., and R.M.S. analyzed data and wrote the paper.

The authors declare no conflict of interest.

This article is a PNAS Direct Submission.

[1]To whom correspondence should be addressed. E-mail: ekz@wustl.edu.

measure isotopic ratios in presolar grains down to less than a micrometer in diameter.

A considerable advance in the study of small grains has been brought about by a new type of ion microprobe, the NanoSIMS (16). This instrument is characterized by a small primary beam spot (down to 50 nm for Cs), high secondary ion transmission at high mass resolution (needed for separation of atomic ions from molecular interferences), and up to seven detectors. The NanoSIMS has played an essential role in the discovery of presolar silicates (17, 18). Although presolar silicates in primitive meteorites are more abundant than other presolar grain species such as SiC, graphite, corundum, and spinel (14, 15), presolar silicates are small (typically 250–300 nm in diameter) and have to be detected in the presence of an overwhelming number of isotopically normal silicates of SS origin. This makes it necessary to measure the isotopic compositions of thousands and tens of thousands of grains, achieved by isotopic raster imaging. Fig. 1 shows O-isotopic ratio images of a 10-μm × 10-μm area covered with small grains from the Acfer 094 primitive meteorite (18). One grain is identified by its anomalous isotopic compositions (excess in ^{17}O and deficit in ^{18}O). Its enlarged SEM image is also shown.

Isotopic imaging in the ion microprobe has been used for the detection of rare grain types such as SiC grains of type X, which have ^{28}Si excesses, indicating an SN origin (19). Even rarer are SiC grains with large ^{29}Si and ^{30}Si excesses, also believed to have an SN origin. Recent automatic imaging with the NanoSIMS identified such grains, and their isotopic ratios provide information on SN nucleosynthesis (20).

Isotopic raster imaging in the NanoSIMS has identified D- and ^{15}N-rich hotspots, small areas with extremely large D and ^{15}N excesses in organic matter from primitive meteorites (21) and in primitive IDPs (22, 23). These excesses indicate the presence of material from the presolar molecular cloud. Primitive IDPs not only have hotspots but also bulk enrichments in ^{15}N as well as high abundances of presolar grains (silicates and SiC). The last study (23) is especially interesting, because in addition to the NanoSIMS, it applies the TEM, Raman microprobe, and X-ray absorption near-edge structure (XANES; see below) to the analysis of IDPs believed to have originated from the comet 26P/Grigg-Skjellerup.

The ion microprobe has also been important in the analysis of material returned from the comet Wild 2 by the Stardust mission. The NanoSIMS was used to identify true O-rich stardust material in impact craters on Al foil (24) and a presolar SiC grain in an aerogel capture cell (25). Ion microprobe oxygen isotopic analysis of Inti, a refractory inclusion captured by Stardust, showed a ^{16}O-rich composition (26), confirming its similarities to CAIs. The presence of a refractory inclusion formed in the inner SS in a comet from the Kuiper belt indicates mixing of material from the inner to the outer solar nebula. Another piece of evidence confirming mixing was obtained by the ion-probe analysis of chondrule-like objects in cometary material from Stardust, which had O-isotopic compositions similar to those of chondrules from carbonaceous chondrites (27).

With large-radius ion microprobes and multidetection with FC, a precision approaching that of thermo-ionization mass spectrometry (TIMS) or inductively coupled plasma-source MS equipped with multiple collectors (MC-ICP-MS) has been achieved, whereas the primary beam diameter is still only ~25 μm (28). Such measurements on chondrules have established that ^{26}Al was uniformly distributed in the early SS, which can be used as a fine-scale chronometer for early SS events (28, 29). A noteworthy technical advance with large-radius ion microprobes that have direct ion imaging capability, such as the Cameca ISM 1270/1280, has been the stacked CMOS-type active pixel sensor (SCAPS). This device allows one to obtain high-spatial resolution isotopic images with high sensitivity. It has not only been successfully used in the search for presolar silicates (30), but it has also led to the discovery of a reservoir extremely enriched in ^{17}O and ^{18}O in the early SS (31).

The MegaSIMS combines SIMS and accelerator MS (AMS). Its main design characteristic is not high lateral spatial resolution but high depth resolution and utmost sensitivity (32, 33). It was especially built for the isotopic analysis of solar wind N and O implanted into samples exposed during the Genesis mission (6). Because solar wind ions are implanted at shallow depth and low fluence, high depth resolution and sensitivity are extremely important. MegaSIMS analysis of Genesis samples has established the N- and O-isotopic compositions of the Sun (34, 35). Both have been the topic of intense debate for decades (36, 37).

Laser Ablation Gas MS

The Sun's N-isotopic composition obtained with the MegaSIMS agrees with that obtained by laser ablation gas MS (LA-GMS), where the solar wind-implanted N was excavated layer by layer by UV laser pulses (38). This technique was also used for the analysis of noble gases in Genesis samples (39). If differs from IR laser bombardment, where sample heating leads to the release of noble gases and where no depth profiles can be obtained. An example is the analysis of He and Ne in cometary matter from Stardust (40).

Auger EM

Although the electron beam used for X-ray analysis in the electron microprobe or SEM can be focused into a very small spot of only a few nanometers, the size of the volume from which X-rays are emitted is typically 1 μm in size. This is much larger than the typical size of presolar silicate grains identified by isotopic imaging in the NanoSIMS. Auger electrons, in contrast, are detected only from the top few nanometers of the sample and can be used for elemental analysis on this spatial scale (41, 42). Thus, Auger EM (AEM) is the ideal complement to the NanoSIMS for the in situ elemental analysis of submicrometer grains.

RIMS

One of the limitations of SIMS is that, generally, it cannot separate isobaric interferences (e.g., ^{92}Zr from ^{92}Mo). One of the great advantages of RIMS is that it uses a finely tuned laser beam to selectively ionize the neutral atoms of a given element sputtered from the sample by an ion beam or desorbed by a laser pulse (43, 44). These ions are then analyzed for their masses in a time of flight (TOF) mass spectrometer. The other advantage is that a large fraction (up to 50%) of the atoms released from the sample can be ionized and detected.

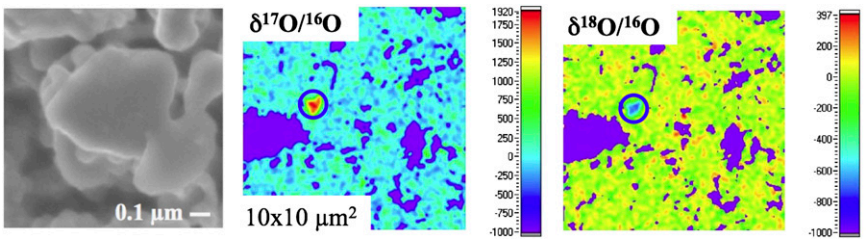

Fig. 1. Isotopic ratio images of O calculated from isotopic raster images obtained with the NanoSIMS. An enlarged SEM picture of a presolar silicate identified from the isotopic images is also shown. Modified from Nguyen and Zinner (18).

These features have been used to measure the Mo- and Zr-isotopic compositions of presolar SiC grains (45). Fig. 2 shows the Mo-isotopic patterns of two presolar SiC grains, identified by their C-, N-, and Si-isotopic ratios as originating from an AGB star (mainstream grain) and a supernova (type X grain) (46). The patterns of these two grains are completely different, indicating different nucleosynthetic processes (s process and neutron pulse, respectively). Another important RIMS result is the identification of the initial presence of ^{99}Tc in presolar SiC grains (47). The detection of Tc, which does not have any stable isotopes, in stars (48) played an important role in the history of the theory of nucleosynthesis (49).

Microprobe Two-Step Laser MS

A variation of RIMS that is applied to the analysis of organic molecules is microprobe two-step laser MS (μL^2MS). In this technique, a whole family of organic compounds desorbed from the sample with a pulsed IR laser beam is ionized resonantly by a UV laser beam. For example, UV light with a wavelength of 266 nm results in electronic excitation of the aromatic ring so that aromatic compounds can be selectively ionized in this way. The detailed masses of these compounds are determined in a TOF mass spectrometer. This techniques has led to the identification of polycyclic aromatic hydrocarbons (PAHs) and alkylated derivatives in IDPs (50) and PAHs in presolar graphite grains (51). Recently, it has resulted in the identification of N-rich aromatic compounds in cometary samples from Stardust (52), similar to what is observed in IDPs. This finding is consistent with the belief that some IDPs have a cometary origin.

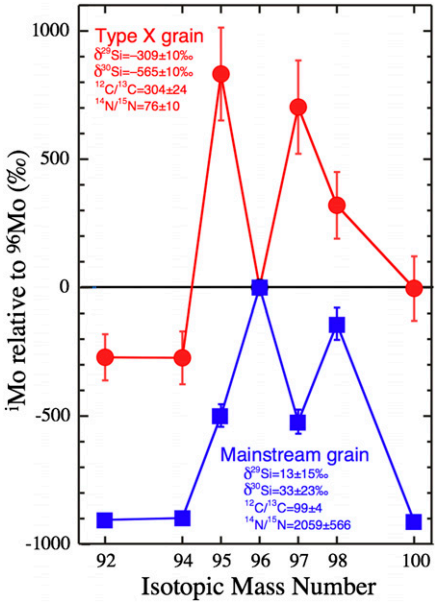

Fig. 2. Molybdenum isotopic patterns measured by RIMS in two different presolar SiC grains. The C-, N-, and Si-isotopic ratios of these grains are also given. Modified from Pellin et al. (46).

AMS

In AMS, negative ions typically produced by sputtering are accelerated to energies of a few MeV and sent through a stripping foil or gas cell, which turns them into positive ions that subsequently go through a magnetic sector mass spectrometer. The outstanding characteristic of this technique is the extreme sensitivity to rare (radioactive) isotopes in the presence of high abundances of other (stable) isotopes. One of the most exciting discoveries by AMS is the detection of the radioisotope ^{60}Fe in deep-sea samples deposited 2.8 Myr ago (53). This finding indicates a nearby SN explosion a few million years ago.

TEM

TEM enables analysis of grain structure, elemental composition, and local bonding at scales ranging from micrometers to subnanometers. TEM images are formed from electrons transmitted through a thin sample (<200 nm) illuminated with high-energy electrons (usually 200 or 300 keV). The contrast in a given image depends on the electron beam illumination conditions (e.g., parallel or focused probe) and the selection of transmitted electrons that have undergone specific kinds of interactions with the sample (e.g., diffraction, high-angle scattering, or inelastic scattering). The most common types of TEM images in cosmochemistry studies are bright-field TEM (BF-TEM) for determination of microstructure, high-resolution TEM (HR-TEM) for imaging of lattice structure and atomic planes, selected area electron diffraction (SAED) for crystal structure determination, scanning TEM annular dark field (STEM-ADF) for atomic number contrast, and energy loss-filtered TEM (EF-TEM) for elemental mapping. In addition to imaging, TEM analysis often includes two types of spectroscopy: energy dispersive X-ray spectroscopy (EDX) and electron energy loss spectroscopy (EELS); both provide elemental composition data, and in the latter case, they also provide information about bond configurations and oxidation states. More details of these techniques can be found in Williams and Carter (54). Applications of EELS are also discussed herein along with the related synchrotron-based XANES analysis.

The structural and chemical data obtained from TEM have fundamentally changed our understanding of the conditions of formation and alteration of SS and extrasolar materials. Studies of presolar grains provide direct constraint on circumstellar dust condensation conditions including temperature, pressure, order of phases condensed, and deviations from thermodynamic equilibrium (55–58) (Fig. 3). For SS materials, such as the Stardust comet Wild 2 samples, TEM data regarding crystallinity and the presence of subgrains inform our understanding of both nebular condensation conditions and radial transport processes (4, 59). Signatures of shock as well as thermal, aqueous, and radiation processing can all be identified. As the quality of electron optics and stability of the electron emitters in transmission electron microscopes has improved, the ability to detect ever more subtle processing signatures has also improved. Field emission sources, aberration-corrected lenses, and monochromation now permit detection of signatures as minute as single-atom impurities in some cases (60, 61).

Focused Ion-Beam Microscopy

Focused ion-beam microscopy (FIB) addresses the need to prepare TEM samples of very heterogeneous materials (e.g., sections of chondrite matrix or rims associated with chondrules and CAIs) (62, 63) and/or isotopically anomalous or otherwise unique grains ranging in size from microns to submicrons (56, 64). The FIB is similar to an SEM with a Ga^+ ion beam in place of the electron beam (FIB) or in combination with an electron beam (FIB-SEM) (65). The user controls the Ga^+ beam current and raster pattern to remove sample material by sputtering and

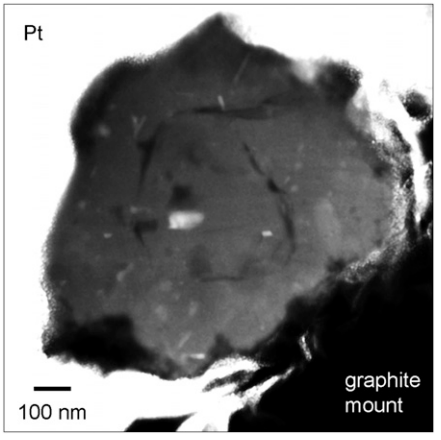

Fig. 3. Scanning TEM annular dark-field (STEM-ADF) image of a type-Z presolar SiC grain. The grain was first isolated from the host meteorite by physical disaggregation and then, was sectioned by focused ion-beam microscopy to form an electron transparent section (123). The STEM-ADF image reveals a crack that extends from the grain surface into the interior as well abundant subgrains. Energy dispersive X-ray spectroscopy (EDX) shows that the crack is oxidized and that the subgrains include multiple phases, some rich in Fe and Ni and others rich in Ti and V.

creates a site-specific electron transparent membrane. The membrane is then extracted from the sample and attached to a TEM support grid by in situ or ex situ micromanipulation for subsequent TEM, SIMS, or XANES analysis. Needle-shaped specimens for atom probe tomography can also be produced.

Atom Probe Tomography

Atom probe tomography is a time of flight MS method for atom by atom tomographic reconstruction of needle-shaped specimens (66). Atoms are evaporated from the needle tip by a combination of applied high-voltage and pulsed laser heating and are collected with a 2D position sensitive detector. Using an estimate of the radius of curvature of the needle tip (50–150 nm) and the TOF and position of a detected atom, the mass and the original location of the atom in the specimen can be determined. Recent atom probe measurements of SiC grains show promise for characterization of trace element segregation in presolar grains that could result from heterogeneous nucleation or ion implantation of circumstellar or interstellar gas (67, 68). Preparation of samples that evaporate uniformly is the major challenge in all atom probe experiments. Needles of pure metal specimens can be obtained by electrochemical etching, but most samples are now prepared by FIB techniques.

Analysis with Synchrotron Radiation

The installation of third-generation electron storage rings specifically designed for the production of synchrotron radiation resulted in new capabilities for microanalysis. In these facilities, high-intensity X-rays are produced by insertion devices (wigglers and undulators) in the path of the electron beam and after selection of a small energy range by a monochromator, can be focused down to diameters of <1 μm by microfocusing mirrors (69). This makes the high-sensitivity analysis of small samples possible. There are several analytical techniques making use of synchrotron radiation (70) that have been applied to extraterrestrial samples. Among the techniques are XRF, X-ray computed microtomography (XRCMT), X-ray diffraction (XRD), X-ray absorption fine structure (XAFS), and XANES.

XRF Analysis. In synchrotron XRF analysis, the (usually monochromatic) finely focused X-rays are used to produce characteristic X-rays from the sample, which are analyzed for their energy, giving information on the elemental composition of the sample (71). Because of the atomic charge (Z) dependence of fluorescence, XRF is especially suited to the analysis of heavier elements. Element images can be obtained by raster scanning. This method has been successfully applied to determine the location and composition of cometary fragments along dust particle tracks in Stardust aerogel (72, 73). These studies found compositional differences between the debris along tracks and terminal particles. Cluster IDPs, analyzed in a similar way, might be an analog to cometary particles collected by Stardust (74). An impressive SXRF study is the measurement of trace element abundances in individual presolar SiC grains ~2 μm in size, providing evidence that the short-lived isotope ^{93}Zr had condensed into the grains at the time of their formation (75).

XRCMT. The 3D internal structure of an object can be obtained by combining many X-ray images, usually by rotating the sample (71, 76). Images of X-ray attenuation yield 3D density structure. This technique has been applied to determine the location and size of cometary particle fragments in Stardust aerogel tracks (77, 78). X-ray tomography can also be done from XRF images and thus, provides the 3D distribution of different elements. However, this analysis requires a pencil beam and is much more time intensive.

Synchrotron Fourier Transform Infrared Spectroscopy. The use of infrared light from synchrotron light sources leads to an increase in brightness of 100–1,000 times over conventional IR sources and allows imaging with diffraction-limited beam spots. The achieved high sensitivity is instrumental for the analysis of small samples such as volatile cometary material deposited in aerogel tracks from the Stardust mission, allowing for the identification of several organic compounds such as amines and amino acids (79, 80).

XANES. Synchrotron XANES (81) and TEM-based electron loss near-edge spectroscopy (ELNES) (82) probe the energy-level structure of atoms in a material. In XANES, the absorption of a monochromated, synchrotron X-ray source because of excitation of electrons from an inner shell is measured as a function of energy. In ELNES, a type of TEM-EELS, the intensity of inelastic scattering of the incident electron beam by the sample because of core-level excitation is measured as a function of the energy loss. Both techniques are commonly used in cosmochemistry to determine oxidation states of Fe (83–85), Ti (25, 86), and other transition metals and to fingerprint carbon bond distributions (87) (e.g., graphite vs. diamond vs. different organic molecules) to constrain formation conditions. In general, soft X-ray XANES has greater sensitivity and energy resolution (<0.1 eV) than does most ELNES (1 eV) because of the bright monochromated X-ray source. Soft X-rays are also less damaging to many materials, particularly organics, than high-energy electrons. Hard X-ray XANES can be used to characterize thicker samples with ~1 eV energy resolution, including submicron particles captured in aerogel (85). However, the achievable spatial resolution of ELNES (subnanometer) is much greater than that of XANES (>10 nm), and 0.1 eV energy resolution can be achieved in a monochromated electron microscope (60, 88).

Raman Microprobe

Raman spectroscopy gives information on molecular bonds, and the Raman microprobe allows analysis on a submicrometer level. It has been successfully applied to the study of insoluble organic matter in primitive meteorites (89), where it was found that metamorphic processes and radiation affect the Raman signal to the identification of ultra-primitive IDPs (23) (see above), the analysis of returned Stardust samples (90), and presolar SiC grains (91). In the last study, the Raman spectrum of a supernova grains indicates crystallographic disorder, whereas grains from AGB stars have a well-crystallized cubic structure.

NMR Spectroscopy

Meteorites and IDPs contain organic material, some of which might have a presolar origin. Recently, NMR analysis has been used to determine the structure of organic macromolecules, the insoluble organic matter (IOM). In solid-state NMR spectroscopy, the resonant frequency of a spin one-half nucleus such as ^{1}H or ^{13}C depends on its electronic environment. Thus, an NMR spectrum provides information about the bonding of these nuclei (92). The study of IOM from primitive meteorites revealed many aromatic and aliphatic functional groups as well as diamond (92, 93). It was found that the relative abundances of aromatic and aliphatic carbon as well as nanodiamonds vary with meteorite group and might provide information on the oxidative nature of aqueous fluids on the meteorites' parent bodies.

ICP-MS

The mid-1990s saw the development of ICP-MS equipped with multiple collectors (MC-ICP-MS). ICP sources can ionize most elements and have permitted the precise isotopic measurement of elements, such as transition metals W, Hf, and Zr, which are poorly ionized by the state of the art TIMS. Because of rapid sample throughput and because the instrumental mass bias varies smoothly during an analytical session, the correction of the instrumental mass bias can be made with an element different from the one being

analyzed (e.g., Cu for Zn) and by bracketing standards (94). The combination of laser ablation with MC-ISP-MS has permitted precise in situ measurements of Mg- and Si-isotopic ratios (95, 96).

During the last 15 y, MC-ICP-MS has become one of the most important techniques in isotope geochemistry and cosmochemistry laboratories. Here, we focus on high-precision MC-ICP-MS isotopic analyses that have led to breakthrough discoveries in cosmochemistry.

Isotopic Heterogeneity in the Solar Nebula. The presence of presolar grains in primitive meteorites is evidence for incomplete homogenization of presolar material during SS formation. Although presolar grain can be analyzed individually, recent improvements in analytical methods and instrumentation, notably MC-ICP-MS, have permitted resolution of small isotopic heterogeneities for several elements in bulk meteorites (e.g., Ti and Ni) (97–99), whereas Fe and Zn have uniform isotopic compositions (100, 101). Measuring the abundance of several isotopes produced by the same process provides useful constraints on the nucleosynthetic processes responsible for the isotopic anomalies. In addition, correlated isotopic effects are used to quantify homogeneity in the SS distribution of extinct radionuclides (e.g., ^{60}Fe $T_{1/2}$ = 1.5 Myr) that could possibly be used as chronometers. For instance, ^{58}Fe and ^{60}Fe are synthesized together in core collapse supernovae or AGB stars by neutron capture reactions (102). Correlated isotopic anomalies of ^{50}Ti, ^{54}Cr, ^{62}Ni, and ^{64}Ni (97–99, 103) have been observed in meteorites and suggest some large-scale isotopic heterogeneity that has survived mixing within the solar nebula. However, the absence of ^{58}Fe-isotopic anomalies larger than 0.3–0.5 ε in bulk meteorites argues for the injection of ^{60}Fe in the early SS and its homogenization before the formation of planetary bodies (100).

Tungsten Isotopes: Age of the Metal/Silicate Differentiation on Earth and Asteroids and the Giant Impact as the Origin of the Moon. Although W is a moderately siderophile element, Hf is a lithophile element and is strongly fractionated from W during core formation. ^{182}Hf/^{182}W chronometry can date Hf/W fractionations that occurred up to ∼60 Myr after the formation of ^{182}Hf (half-life = 9 Myr). Comparison of terrestrial mantle samples with chondrites has been used to evaluate the timing of terrestrial core formation (104–107). Although Lee and Halliday (105) did not find any difference in the W-isotopic composition between terrestrial samples and chondrites, later studies detected a small but resolvable ∼20 ppm excess of ^{182}W in the Earth relative to chondrites (106–108). These results imply that core mantle differentiation occurred probably within 30 Myr after SS formation.

Iron meteorites, thought to represent the core of asteroids, have deficits of 3–5 ε in ^{182}W/^{184}W ratio compared with terrestrial samples (109–112). These deficits correspond to differentiation ages of ∼1–5 Myr after SS formation. The first Pb-Pb dating of Group IVA iron meteorites confirmed this rapid differentiation of iron meteorite parent bodies (113).

The silicate fraction of the Moon has the same ^{182}W/^{184}W ratio as the Earth's mantle (114). The implications of this result on the time of the giant impact as the origin of the Moon depend on its Hf/W ratio. A higher than terrestrial Hf/W ratio, derived from the W/U ratio of lunar rocks (114), implies a time for the giant impact >60 Myr after SS formation. However, Yin et al. and Yin and Antognini (115, 116) argued that the Hf/W ratios of the two planetary bodies were similar, reducing the time to ∼30 Myr, as initially suggested (106, 107).

Variations of Stable Isotopes of Heavy Elements: Tracers of SS Processes. Small stable isotopic fractionations of heavy elements have been measured by MC-ICP-MS in meteorites and lunar samples for moderately volatile elements (e.g., Zn and Cd) (117, 118) and more refractory elements (e.g., Fe and Ni) (119, 120). These isotopic variations, which are too small to be measured by any other instrument, brought additional constraints on the volatile history and the physical processes (e.g., impacts), which have modified the meteorite parent bodies and the Earth. The abundance of Zn, a moderately volatile element, in carbonaceous chondrites decreases in this order: CI > CM > CV-CO > Earth (121). Its isotopic composition decreases in the same order from isotopically heaviest in CIs to isotopically lightest in the Earth (117). The opposite pattern is expected if the Zn depletion in Zn in chondrites and Earth relative to CI chondrites is because of volatilization. The observed pattern is an argument in favor of an incomplete accretion origin for the volatile depletion in the SS (122).

ACKNOWLEDGMENTS. We thank Steve Sutton for providing information on synchrotron radiation analysis. This work was supported by National Aeronautics and Space Administration Funds NNX08AG71G (to E.K.Z.), NNX09AM64G (to F.M.), and NNH09AL20I (to R.M.S.).

1. Maurette M (2006) *Micrometeorites and the Mysteries of our Origins* (Springer, Heidelberg).
2. Brownlee DE (1985) Cosmic dust: Collection and research. *Annu Rev Earth Planet Sci* 13:147–173.
3. Bradley JP (2004) Interplanetary dust particles. *Meteorites, Planets, and Comets: Treatise on Geochemistry*, eds Holland HD, Turekian KK (Elsevier-Pergamon, Oxford), Vol 1, pp 689–711.
4. Brownlee D, et al. (2006) Comet 81P/Wild 2 under a microscope. *Science* 314:1711–1716.
5. Yano H, et al. (2006) Touchdown of the Hayabusa spacecraft at the Muses Sea on Itokawa. *Science* 312: 1350–1353.
6. Burnett DS, et al. (2003) The Genesis discovery mission: Return of solar matter to earth. *Space Sci Rev* 105:509–534.
7. Clayton RN, Grossman L, Mayeda TK (1973) A component of primitive nuclear composition in carbonaceous meteorites. *Science* 182:485–488.
8. Lee T, Panastassiou DA, Wasserburg GJ (1976) Demonstration of ^{26}Mg excess in Allende and evidence for ^{26}Al. *Geophys Res Lett* 3:109–112.
9. Wasserburg GJ (1987) Isotopic abundances: Inferences on solar system and planetary evolution. *Earth Planet Sci Lett* 86:129–173.
10. Westphal AJ, et al. (2004) Aerogel keystones: Extraction of complete hypervelocity impact events from aerogel collectors. *Meteorit Planet Sci* 39:1375–1386.
11. (2008) *Meteorit Planet Sci* 43(1–2).
12. Zinner E (1989) Isotopic measurements with the ion microprobe. *New Frontiers in Stable Isotope Research: Laser Probes, Ion Probes, and Small-Sample Analysis*, eds Shanks WC, III, Criss RE (US Geological Survey), US Geological Survey Bulletin 1890, pp 145–162.
13. Ireland TR (2003) SIMS measurement of stable isotopes. *Handbook of Stable Isotope Analytical Techniques*, ed de Groot PA, pp 652–691.
14. Clayton DD, Nittler LR (2004) Astrophysics with presolar stardust. *Annu Rev Astron Astrophys* 42: 39–78.
15. Zinner E (2007) Presolar grains. *Treatise on Geochemistry Update*, eds Holland HD, Turekian KK, Davis A (Elsevier Ltd, Oxford), Vol 1.02, pp 1–33.
16. Hillion F, Horreard F, Stadermann FJ (2000) Recent results and developments on the CAMECA NanoSIMS 50. *Proceedings of the 12th International Conference on Secondary Ion Mass Spectrometry* (John Wiley & Sons, Brussels), pp 209–212.
17. Messenger S, Keller LP, Stadermann FJ, Walker RM, Zinner E (2003) Samples of stars beyond the solar system: Silicate grains in interplanetary dust. *Science* 300:105–108.
18. Nguyen AN, Zinner E (2004) Discovery of ancient silicate stardust in a meteorite. *Science* 303:1496–1499.
19. Nittler LR, et al. (1995) Silicon nitride from supernovae. *Astrophys J* 453:L25–L28.
20. Hoppe P, et al. (2010) NanoSIMS studies of small presolar SiC grains: New insights into supernova nucleosynthesis, chemistry, and dust formation. *Astrophys J* 719:1370–1384.
21. Busemann H, et al. (2006) Interstellar chemistry recorded in organic matter from primitive meteorites. *Science* 312:727–730.
22. Floss C, et al. (2006) Identification of isotopically primitive interplanetary dust particles: A NanoSIMS isotopic imaging study. *Geochim Cosmochim Acta* 70: 2371–2399.
23. Busemann H, et al. (2009) Ultra-primitive interplanetary dust particles from the comet 26P/Grigg-Skjellerup dust stream collection. *Earth Planet Sci Lett* 288:44–57.
24. Stadermann FJ, et al. (2008) Stardust in Stardust—the C, N, and O isotopic compositions of Wild 2 cometary matter in Al foil impacts. *Meteorit Planet Sci* 43: 299–313.
25. Messenger S, et al. (2009) Discovery of presolar SiC from Comet WILD-2. *Lunar Planet Sci* 40:1790.
26. Simon SB, et al. (2008) A refractory inclusion returned by Stardust from comet 81P/Wild 2. *Meteorit Planet Sci* 43:1861–1877.
27. Nakamura T, et al. (2008) Chondrulelike objects in short-period comet 81P/Wild 2. *Science* 321:1664–1667.
28. Villeneuve J, Chaussidon M, Libourel G (2009) Homogeneous distribution of ^{26}Al in the solar system from the Mg isotopic composition of chondrules. *Science* 325:985–988.

29. MacPherson GJ, et al. (2010) Early solar nebula condensates with canonical, not supracanonical, initial $^{26}Al/^{27}Al$ ratios. *Astrophys J* 711:L117–L121.
30. Nagashima K, Krot AN, Yurimoto H (2004) Stardust silicates from primitive meteorites. *Nature* 428: 921–924.
31. Sakamoto N, et al. (2007) Remnants of the early solar system water enriched in heavy oxygen isotopes. *Science* 317:231–233.
32. Mao PH, et al. (2005) Preliminary evaluation of the secondary ion/accelerator mass spectromer, MegaSIMS. *Lunar Planet Sci* 36:2259.
33. Mao PH, et al. (2006) MegaSIMS update: Oxygen transmission, destruction of OH molecular ions, and stability of three-isotope measurements. *Lunar Planet Sci* 37:2153.
34. Kallio APA, et al. (2010) Nitrogen isotopic composition of solar wind returned by the Genesis mission. *Lunar Planet Sci* 41:2481.
35. McKeegan KD, et al. (2010) Genesis SiC concentrator sample traverse: Confirmation of 16O-depletion of terrestrial oxygen. *Lunar Planet Sci* 41:2589.
36. Owen T, et al. (2001) Protosolar nitrogen. *Astrophys J* 553:L77–L79.
37. Wiens RC, Huss GR, Burnett DS (1999) The solar oxygen-isotopic composition: Predictions and implications for solar nebula processes. *Meteorit Planet Sci* 34:99–107.
38. Marty B, et al. (2010) Nitrogen isotopes in the recent solar wind from the analysis of Genesis targets: Evidence for large scale isotope heterogeneity in the early solar system. *Geochim Cosmochim Acta* 74: 340–355.
39. Meshik A, et al. (2007) Constraints on neon and argon isotopic fractionation in solar wind. *Science* 318: 433–435.
40. Marty B, et al. (2008) Helium and neon abundances and compositions in cometary matter. *Science* 319: 75–78.
41. Floss C, et al. (2010) A NanoSIMS and Auger Nanoprobe investigation of an isotopically primitive interplanetary dust particle from the 55P/Tempel-Tuttle targeted stratospheric dust collector. *Meteorit Planet Sci* 45:1889–1905.
42. Stadermann FJ, et al. (2009) The use of Auger spectroscopy for the in situ elemental characterization of sub-micrometer presolar grains. *Meteorit Planet Sci* 44:1033–1049.
43. Savina MR, et al. (2003) Analyzing individual presolar grains with CHARISMA. *Geochim Cosmochim Acta* 67: 3215–3225.
44. Levine J, et al. (2009) Resonance ionization mass spectrometry for precise measurements of isotope ratios. *Int J Mass* 288:36–43.
45. Lugaro M, et al. (2003) Isotopic compositions of strontium, zirconium, molybdenum, and barium in single presolar SiC grains and asymptotic giant branch stars. *Astrophys J* 593:486–508.
46. Pellin MJ, et al. (1999) Molybdenum isotopic composition of single silicon carbide grains from supernovae. *Lunar Planet Sci* 30:1969.
47. Savina MR, et al. (2004) Extinct technetium in presolar silicon carbide grains. *Science* 303:649–652.
48. Merrill PW (1952) Spectroscopic observations of stars of class S. *Astrophys J* 116:21–26.
49. Burbidge EM, et al. (1957) Synthesis of the elements in stars. *Rev Mod Phys* 29:547–650.
50. Clemett SJ, Maechling CR, Zare RN, Swan PD, Walker RM (1993) Identification of complex aromatic molecules in individual interplanetary dust particles. *Science* 262:721–725.
51. Messenger S, et al. (1998) Indigenous polycyclic aromatic hydrocarbons in circumstellar graphite grains from primitive meteorites. *Astrophys J* 502: 284–295.
52. Clemett SJ, et al. (2010) Complex aromatic hydrocarbons in Stardust samples collected from comet 81P/Wild 2. *Meteorit Planet Sci* 45:701–722.
53. Knie K, et al. (2004) 60Fe anomaly in a deep-sea manganese crust and implications for a nearby supernova source. *Phys Rev Lett* 93:171103-1–171103-4.
54. Williams DB, Carter CB (2008) *Transmission Electron Microscopy: A Textbook for Materials Science* (Springer, New York).
55. Bernatowicz TJ, et al. (1996) Constraints on stellar grain formation from presolar graphite in the murchison meteorite. *Astrophys J* 472:760–782.
56. Stroud RM, Nittler LR, Alexander CMOD (2004) Polymorphism in presolar Al_2O_3 grains from asymptotic giant branch stars. *Science* 305:1455–1457.
57. Vollmer C, et al. (2009) Direct laboratory analysis of silicate stardust from red giant stars. *Astrophys J* 700: 774–782.
58. Messenger S, Keller LP, Lauretta DS (2005) Supernova olivine from cometary dust. *Science* 309:737–741.
59. Ishii HA, et al. (2008) Comparison of comet 81P/Wild 2 dust with interplanetary dust from comets. *Science* 319:447–450.
60. Bradley JP, Dai ZR (2009) Analytical SuperSTEM for extraterrestrial materials research. *Meteorit Planet Sci* 44:1627–1642.
61. Krivanek OL, et al. (2010) Atom-by-atom structural and chemical analysis by annular dark-field electron microscopy. *Nature* 464:571–574.
62. Zega TJ, et al. (2007) Coordinated isotopic and mineralogic analyses of planetary materials enabled by in situ lift-out with a focused ion beam scanning electron microscope. *Meteorit Planet Sci* 42: 1373–1386.
63. Graham GA, et al. (2008) Applied focused ion beam techniques for sample preparation of astromaterials for integrated nanoanalysis. *Meteorit Planet Sci* 43: 561–569.
64. Leroux H, et al. (2008) Transmission electron microscopy of cometary residues from micron-sized craters in the Stardust Al foils. *Meteorit Planet Sci* 43: 143–160.
65. Giannuzzi LA, Stevie FA (2005) *Introduction to Focused Ion Beams: Instrumentation, Theory, Techniques, and Practice* (Springer, New York).
66. Kelly TF, Miller MK (2007) Invited review article: Atom probe tomography. *Rev Sci Instrum* 78:031101–031129.
67. Heck PR, et al. (2010) Atom-probe tomographic analyses of presolar silicon carbide grains and meteoritic nanodiamonds—first results on silicon carbide. *Lunar Planet Sci* 41:2112.
68. Stadermann FJ, et al. (2010) Atom-probe tomographic study of the three-dimensional structure of presolar silicon carbide and nanodiamonds at atomic resolution. *Lunar Planet Sci* 41:2134.
69. Sham TK, Rivers ML (2002) A brief overview of synchrotron radiation. *Rev Miner Geochem* 49: 118–147.
70. Brown J, G E, Sturchio NC (2002) An overview of synchrotron radiation applications to low temperature geochemistry and environmental science. *Rev Miner Geochem* 49:1–115.
71. Sutton SR, et al. (2002) Microfluorescence and microtomography analyses of heterogeneous earth and environmental materials. *Rev Miner Geochem* 49: 429–483.
72. Lanzirotti A, et al. (2008) Chemical composition and heterogeneity of Wild 2 cometary particles determined by synchrotron x-ray fluorescence. *Meteorit Planet Sci* 43:187–214.
73. Ishii HA, et al. (2008) Recovering the elemental composition of comet Wild 2 dust in five Stardust impact tracks and terminal particles in aerogel. *Meteorit Planet Sci* 43:215–231.
74. Flynn GJ, Lanzirotti A, Sutton SR (2009) Elemental and mineralogical compositions of cluster IDPs: A possible analog of the Wild 2 particles collected by Stardust. *Lunar Planet Sci* 40:1166.
75. Kashiv Y, et al. (2010) Extinct ^{93}Zr in single presolar SiC grains from low mass asymptotic giant branch stars and condensation from Zr-depleted gas. *Astrophys J* 713:212–219.
76. Ebel D, Rivers ML (2007) Meteorite 3-D synchrotron microtomography: Methods and applications. *Meteorit Planet Sci* 42:1627–1646.
77. Tsuchiyama A, et al. (2009) Three-dimensional structures and elemental distributions of Stardust impact tracks using synchrotron microtomography and X-ray fluorescence analysis. *Meteorit Planet Sci* 44:1203–1224.
78. Ebel DS, et al. (2009) Three-dimensional textural and compositional analysis of particle tracks and fragmentation history in aerogel. *Meteorit Planet Sci* 44:1445–1463.
79. Sandford SA, et al. (2006) Organics captured from comet 81P/Wild 2 by the Stardust spacecraft. *Science* 314:1720–1724.
80. Bajt S, et al. (2009) Infrared spectroscopy of Wild 2 particle hypervelocity tracks in Stardust aerogel: Evidence for the presence of volatile organics in cometary dust. *Meteorit Planet Sci* 44:471–484.
81. Koningsberger DC, Prins R (1988) *X-Ray Absorption: Principles, Applications, Techniques of EXAFS, SEXAFS, and XANES* (Wiley, New York).
82. Egerton RF (1996) *Electron Energy-Loss Spectroscopy in the Electron Microscope* (Plenum, New York).
83. Zega TJ, Garvie LAJ, Buseck PR (2003) Nanometer-scale measurements of iron oxidation states of cronstedtite from primitive meteorites. *Am Miner* 88:1169–1172.
84. Ogliore RC, et al. (2010) Comparison of the oxidation state of Fe in comet 81P/Wild 2 and chondritic-porous interplanetary dust particles. *Earth Planet Sci Lett* 296: 278–286.
85. Westphal AJ, et al. (2009) Mixing fraction of inner solar system material in comet 81P/Wild 2. *Astrophys J* 694:18–28.
86. Chi M, et al. (2009) The origin of refractory minerals in comet 81P/Wild 2. *Geochim Cosmochim Acta* 73: 7150–7161.
87. Cody GD, et al. (2008) Quantitative organic and light-element analysis of comet 81P/Wild 2 particles using C-, N-, and O-mu-XANES. *Meteorit Planet Sci* 43:353–365.
88. Krivanek OL, et al. (2009) High-energy-resolution monochromator for aberration-corrected scanning transmission electron microscopy/electron energy-loss spectroscopy. *Philos Transact A Math Phys Eng Sci* 367:3683–3697.
89. Busemann H, Alexander CMOD, Nittler LR (2007) Characterization of insoluble organic matter in primitive meteorites by microRaman spectroscopy. *Meteorit Planet Sci* 37:1387–1416.
90. Rotundi A, et al. (2008) Combined micro-Raman, micro-infrared, and field emission scanning electron microscope analyses of comet 81P/Wild 2 particles collected by Stardust. *Meteorit Planet Sci* 43:367–397.
91. Wopenka B, et al. (2010) Raman and isotopic studies of large presolar SiC grains. *Lunar Planet Sci* 41:1390.
92. Cody GD, Alexander CMOD, Tera F (2002) Solid-state (^1H and ^{13}C) nuclear magnetic resonance spectroscopy of insoluble organic residue in the Murchison meteorite: A self-consistent quantititive analysis. *Geochim Cosmochim Acta* 66:1851–1865.
93. Cody GD, Alexander CMOD (2005) NMR studies of chemical structural variation of insoluble organic matter from different carbonaceous chondrite groups. *Geochim Cosmochim Acta* 69:1085–1097.
94. Albarède F, et al. (2004) Precise and accurate isotopic measurements using multiple-collector ICPMS. *Geochim Cosmochim Acta* 68:2725–2744.
95. Shahar A, Young ED (2007) Astrophysics of CAI formation as revealed by silicon isotope LA-MC-ICPMS of an igneous CAI. *Earth Planet Sci Lett* 257:497–510.
96. Young ED, et al. (2005) Supra-canonical $^{26}Al/^{27}Al$ and the residence time of CAIs in the solar protoplanetary disk. *Science* 308:223–227.
97. Leya I, et al. (2008) Titanium isotopes and the radial heterogeneity of the solar system. *Earth Planet Sci Lett* 266:233–244.
98. Trinquier A, et al. (2009) Origin of nucleosynthetic isotope heterogeneity in the solar protoplanetary disk. *Science* 324:374–376.
99. Regelous M, Elliott T, Coath CD (2008) Nickel isotope heterogeneity in the early Solar System. *Earth Planet Sci Lett* 272:330–338.
100. Dauphas N, et al. (2008) Iron 60 evidence for early injection and efficient mixing of stellar debris in the protosolar nebula. *Astrophys J* 686:560–569.
101. Moynier F, Dauphas N, Podosek FA (2009) A Search for ^{70}Zn Anomalies in Meteorites. *Astrophys J* 700: L92–L95.
102. Clayton DD (2003) *Handbook of Isotopes in the Cosmos: Hydrogen to Gallium* (Cambridge University Press, Cambridge, UK).
103. Steele RCJ, et al. (2010) Correlated neutron rich Ni isotope anomalies in chondritic and iron meteorites. *Lunar Planet Sci* 44:1984.
104. Harper CL, Jr., Jacobsen SB (1996) Evidence for ^{182}Hf in the early Solar System and constraints on the

timescale of terrestrial accretion and core formation. *Geochim Cosmochim Acta* 60:1131–1153.
105. Lee DC, Halliday AN (1995) Hafnium-tungsten chronometry and the timing of terrestrial core formation. *Nature* 378:771–774.
106. Kleine T, Münker C, Mezger K, Palme H (2002) Rapid accretion and early core formation on asteroids and the terrestrial planets from Hf-W chronometry. *Nature* 418:952–955.
107. Yin Q, et al. (2002) A short timescale for terrestrial planet formation from Hf-W chronometry of meteorites. *Nature* 418:949–952.
108. Schoenberg R, et al. (2002) New W-isotope evidence for rapid terrestrial accretion and very early core formation. *Geochim Cosmochim Acta* 66:3151–3160.
109. Horan MF, Smoliar MI, Walker RJ (1998) ^{182}W and ^{187}Re-^{187}Os systematics of iron meteorites: Chronology for melting, differentiation, and crystallization in asteroids. *Geochim Cosmochim Acta* 62: 545–554.
110. Markowski A, et al. (2006) Tungsten isotopic compositions of iron meteorites: Chronological constraints vs. cosmogenic effects. *Earth Planet Sci Lett* 242:1–15.
111. Schersten A, et al. (2006) Hf-W evidence for rapid differentiation of iron meteorite parent bodies. *Earth Planet Sci Lett* 241:530–542.
112. Qin L, et al. (2008) Rapid accretion and differentiation of iron meteorite parent bodies inferred from ^{182}Hf-^{182}W chronometry and thermal modeling. *Earth Planet Sci Lett* 273:94–104.
113. Blichert-Toft J, et al. (2010) The early formation of the IVA iron meteorite parent body. *Earth Planet Sci Lett* 296:269–280.
114. Touboul M, Kleine T, Bourdon B, Palme H, Wieler R (2007) Late formation and prolonged differentiation of the Moon inferred from W isotopes in lunar metals. *Nature* 450:1206–1209.
115. Yin Q-Z, Tollstrup D, Wimpenny J (2010) Constraining the timing of giant-impact and the origin of the Earth-Moon system. New advances in lunar exploration. *Proceedings of the International Symposium on Lunar Science*, eds Ouyang Z, Lp WH, Tang Z (Macau University of Science and Technology, Macau), pp 71–91.
116. Yin Q-Z, Antognini J (2008) Isotopic and elemental constraints on the first 100 Myr of earth history. *Geochim Cosmochim Acta* (Suppl 72):A1061.
117. Luck JM, Othman DB, Albarede F (2005) Zn and Cu isotopic variations in chondrites and iron meteorites: Early solar nebula reservoirs and parent-body processes. *Geochim Cosmochim Acta* 69:5351–5363.
118. Wombacher F, et al. (2008) Cadmium stable isotope cosmochemistry. *Geochim Cosmochim Acta* 72: 646–667.
119. Poitrasson F, et al. (2004) Iron isotope differences between Earth, Moon, Mars and Vesta as possible records of contrasted accretion mechanisms. *Earth Planet Sci Lett* 223:253–266.
120. Moynier F, et al. (2007) Comparative stable isotope geochemistry of Ni, Cu, Zn, and Fe in chondrites and iron meteorites. *Geochim Cosmochim Acta* 71: 4365–4379.
121. Lodders K, Fegley B, Jr. (1998) *The Planetary Scientist's Companion* (Oxford University Press, London).
122. Albarède F (2009) Volatile accretion history of the terrestrial planets and dynamic implications. *Nature* 461:1227–1233.
123. Stroud RM, et al. (2003) Transmission electron microscopy of non-etched presolar silicon carbide. *Lunar Planet Sci* 34:1755.